Submitted Manuscript

Applied Spectroscopy

www.s-a-s.org

Effect of Femtosecond Ultraviolet and Infrared Laser Wavelength on Plasma Characteristics of Metals, Ceramics and Glass Samples Using Femtosecond Laser-Induced Breakdown Spectroscopy

Applied Spectroscopy
2024, Vol. 78(6) 579–590

DOI: 10.1177/00037028241240782
journals.sagepub.com/home/asp
Sage

Gytis Zaremba[1], Domas Paipulas[1], Virgilijus Vaičaitis[1], and Ona Balachninaite[1]

Abstract

In this work, we present studies on the effect of laser wavelengths on the laser-induced plasma characterization using a femtosecond (fs) ytterbium-doped potassium-gadolinium tungstate (Yb:KGW) laser. Plasma plumes of copper, steel, ceramics, and glass samples were induced using a multiple shot of 200 fs laser pulses with 1030 nm and 343 nm wavelengths at fixed laser fluence (10.5 J/cm^2) and analyzed using the laser-induced breakdown spectroscopy (LIBS) technique. Time-resolved fs-LIBS measurements were performed on the same set of samples and under the same experimental conditions. For the calculation of plasma parameters, the set of spectral lines of Cu(I) (for copper sample), Fe(I) (for steel sample), and Ca(I), K(I) (for glass and ceramics samples) were observed. The plasma electron temperature and density were evaluated from the Boltzmann plots and Stark-broadening profiles of the plasma spectral lines, assuming the local thermodynamic equilibrium condition. Time-resolved plasma temperature and electron density for fs-LIBS using ultraviolet (UV) and infrared (IR) laser wavelengths were analyzed and no significant dependence on fs laser wavelength was observed for any of the samples. However, for all samples the signal-to-noise ratio (SNR) significantly increased using UV laser radiation: copper (~100%), steel (~300%), glass (~400%), and ceramics (~40%). Therefore, by using a fs UV laser wavelength for laser-induced breakdown spectroscopy experiments, for certain materials the SNR and at the same time the limit of detection can be significantly enhanced.

Keywords

Plasma emission, femtosecond laser-induced breakdown spectroscopy, fs-LIBS, femtosecond ultraviolet and infrared LIBS, optical emission spectroscopy, plasma plume, electron density, plasma temperature

Date received: 1 June 2023; accepted: 25 February 2024

Introduction

Laser-induced breakdown spectroscopy (LIBS) is a versatile tool widely used for the elemental analysis of various materials, both in situ and in the laboratory.[1,2] The use of ultrashort femtosecond (fs) pulses for LIBS has many advantages compared to long pulses. One of them is the reduced heat-affected zone, which is proportional to the square root of the pulse duration.[3,4] Other advantages of fs-LIBS are reduced optical continuum emission, generation of colder plasma, less susceptibility to sampling matrix and elemental fractional effects, non-gated detection, better spatial and depth resolution, lower ablation threshold, and better repeatability.[2,5] Fs laser pulses are perfect for remote or stand-off detection because they can form filaments and are able to deliver high energies over long distances. They have been used in remote atmospheric sensing and pollution detection,[6,7] analysis of chemical and biological agents,[8] cultural heritage monitoring,[9] metal analysis,[10] and the detection of explosives,[11,12] etc.[13,14]

An important parameter of LIBS is the laser wavelength used for plasma generation on the sample surface. The dependence of laser-induced plasma parameters on wavelength has been studied before, but mainly using nanosecond laser pulses. Most of the studies presented below used nanosecond laser pulses.

[1]Laser Research Center, Vilnius University, LT, Vilnius, Lithuania

Corresponding author:
Ona Balachninaite, Laser Research Center, Vilnius University, Saulėtekio ave. 10, LT-10223 Vilnius, Lithuania.
Email: ona.balachninaite@ff.vu.lt

Diaz et al.[15] found that the main parameters of LIBS (plasma temperature and electron density) were almost the same for both 1064 and 355 nm wavelengths of the neodymium-doped yttrium aluminum garnet (Nd:YAG) laser using 56 mJ pulse energy on gold- and silver-bearing minerals, but the repeatability of measurements increased by 50% with 355 nm wavelength. There were also other studies that have observed better repeatability with the shorter laser wavelengths.[16–18]

Amoruso et al.[19] evaluated absorption mechanisms in aluminum laser-ablated plasmas, and found that, at the visible laser wavelength (532 nm) of the Nd:YAG laser, in the first stages of the laser–vapor interaction, ionization is mainly caused by an inverse bremsstrahlung process due to electron scattering by neutrals and subsequent collisional ionization, whereas in the ultraviolet (UV), photoionization of excited species plays the most important role. In both cases, the plasma acts as a shield for the laser radiation, thus absorbing a part of the laser pulse.[20] However, shorter pulses (on the order of picoseconds rather than nanoseconds) have been reported to be more effective in ablating the mass, probably because plasma shielding does not have such a strong effect at shorter pulses.[21]

Qaisar and Pert[22] investigated the effect of laser wavelength on the ablation process by comparing UV KrF excimer and infrared Nd:YAG lasers. It was discovered that plasma screening is more effective for longer-wavelength lasers, whereas shorter-wavelength lasers are more beneficial for ablation. Other studies confirm these results.[16,21,23–25] Qaisar and Pert[22] also observed that a longer infrared (IR) wavelength produces a higher temperature but lower density plasma, as compared to shorter UV wavelength-induced plasma. However, Abdellatif and Imam[26] obtained different results, where the UV wavelength of an Nd:YAG laser produced both a higher temperature and higher electron density of the plasma on aluminum, as compared with the IR wavelength.

Kasem et al.[17] established that the use of the UV wavelength of the Nd:YAG laser with 22 mJ pulse energy results in more stable plasma, which gave more realistic elemental results of the archaeological bone plasma than longer IR wavelengths. They also observed that the use of UV laser radiation reduces fractionation effects, which can cause the ratios of the elements in a plume to differ from the stoichiometry of the sample. Other studies confirm these results.[27,28] However, Huber et al.[29] concluded that the IR wavelength is better at finding heavy metal impurities in polymer materials.

Fornarini et al.[30] found that, when using Nd:YAG laser radiation in the UV range for LIBS on bronze samples, there is almost no dependence of the plasma parameters on fluence, which was varied from 50 to 250 J/cm^2, contrary to IR excitation.

Aberkane et al.[31] investigated the influence of a 50 mJ Nd:YAG laser with wavelengths 1064, 532, and 355 nm at 7, 9, and 10 ns pulse durations, respectively, on the relationship between Te and surface hardness of Fe–V–C metallic alloys. They determined that employing an excitation laser in the IR range rather than in the UV range is more efficient for measuring surface hardness using LIBS.

Studies on the effects of an appropriate combination of laser wavelengths and pulse energies on the characterization of generated plasma on a pure copper sample using a single shot picosecond (170 ps) Nd:YAG laser were performed by Fikry et al.[32] It was found that the copper emission line intensities (SNR), plasma temperature, and density show a strong dependence on the laser wavelength and pulse energy. The electron temperature and electron density values gradually increase with the increase of the laser wavelength and pulse fluence. The researchers explained this tendency by the fact that using picosecond pulses enhances the plasma shielding effect, which is due to the inverse Bremsstrahlung being the dominant absorption mechanism, not photoionization. Therefore, most of the laser energy is absorbed by the free electrons of the target, and more energetic electrons are preserved, which causes an increase in the electron temperature and electron density with the increase of the picosecond laser wavelength and pulse energy.

A comparison of mid-infrared (2.05 μm) and infrared (800 nm) wavelength fs (~40 fs) pulses using a Ti:sapphire laser for LIBS on copper was carried out by Hartig et al.[5] A pulse energy of 200 μJ was used. They found that the signal-to-noise ratio (SNR) decreases by ~40% with the use of a longer mid-IR laser wavelength, compared to IR. The overall line intensity was approximately seven times higher after 800 nm laser ablation. Plasma electron density and temperature are also decreased with the longer 2.05 μm laser wavelength, and the authors attribute this decrease to the reduced multi-photon ionization efficiency at longer wavelengths, which then results in less effective laser–matter coupling, lower ablation, and plasma density.

The choice of wavelength for LIBS measurements is thought to be more important for longer pulses, closer to the regime of nanoseconds, but in the case of fs-LIBS, the pulse–matter interaction is different, the pulse duration is much shorter than the material heat transfer time, plasma forms after the pulse, eliminating the problem of plasma shielding. However, the dependence on fs UV and IR LIBS has not been extensively studied.

In this work, two different fs laser wavelengths of 1030 and 343 nm were used to determine the effect of wavelength on LIBS parameters. We found that using both IR and UV laser wavelengths results in plasma of roughly the same temperature, electron density, and intensity of spectral lines, but the SNR is significantly increased using UV laser wavelength for plasma generation.

Experimental Setup

The experimental scheme for our LIBS measurements is shown in Figure 1. In our experiment, we used the "Pharos" fs ytterbium-doped potassium-gadolinium tungstate (Yb:KGW) laser (Light Conversion Ltd.) with a pulse

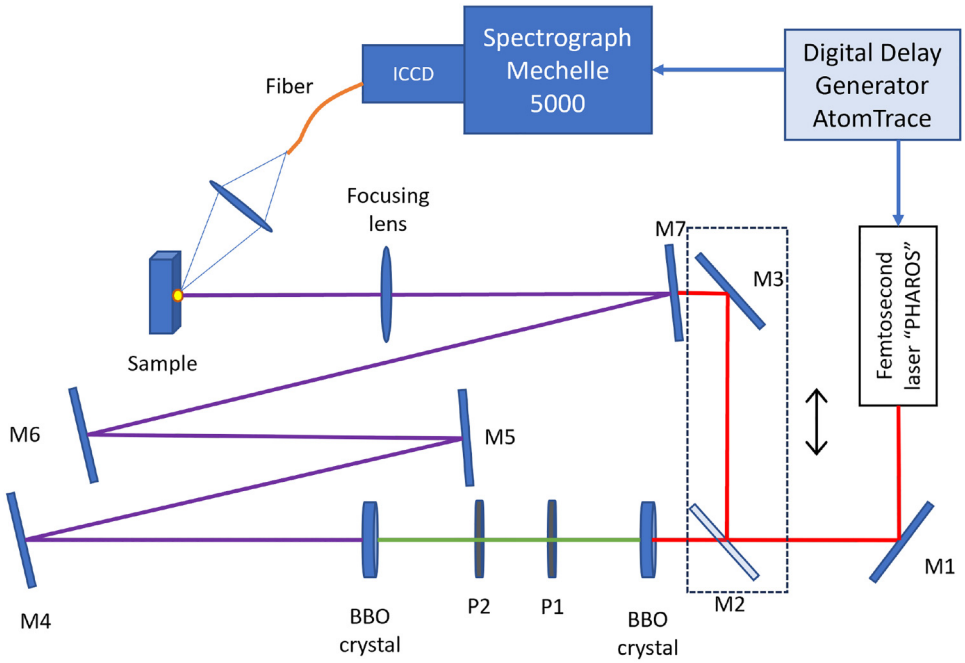

Figure 1. Experimental setup for time-resolved fs-LIBS measurements using 343 and 1030 nm wavelengths. M1–M3 are high-reflective mirrors for the first harmonic and M4–M7 are high-reflective mirrors for the third harmonic and high transmittance for the first and second harmonics (used to eliminate IR and visible laser radiation). P1 and P2 are half waveplate and dispersion compensation elements.

duration of 200 fs, average power up to 6 W at 1030 nm and pulse repetition rate of 6 kHz. The fundamental harmonic (1030 nm) was used for IR radiation. For the generation of UV radiation, the fundamental wavelength was first frequency doubled (515 nm), and then the sum frequency generated (343 nm) using nonlinear beta barium borate crystals. High reflectivity mirrors (for 343 nm) M4–M7 were used to filter out the first (1030 nm) and second (515 nm) harmonics, so that only the third harmonic (343 nm) remained. M1–M3 mirrors were used for the first harmonic and M2–M3 mirrors were used only during the IR laser wavelength experiment. The fluence on the sample using both UV and IR laser wavelengths was kept constant at $10.5 \pm 1.5\,J/cm^2$. The spot size on the sample surface was $29 \pm 2\,\mu m$ with UV and $39 \pm 2\,\mu m$ with IR wavelengths. It was measured using a laser beam profile Newport LBP2 camera and Liu's method (with steel sample used).[33] UV radiation was focused on the sample surface with a 200 mm focal length ultraviolet grade fused silica (UVFS) lens, and IR radiation was focused with 100 mm focal length UVFS lens. The corresponding energies of the fundamental and the third harmonics were chosen to keep the same laser fluences in both cases.

Our samples were copper, oxygen-free high thermal conductivity (99.95+% purity) (Goodfellow Cambridge Ltd.); stainless steel, AISI 301 (Goodfellow Cambridge Ltd.); glass (green optical glass filter; Izium); and a ceramics (Diwali light turquoise plate; Luminarc Ltd.). The elemental analysis of the glass and ceramics samples was performed with the wavelength dispersive X-ray fluorescence (WDXRF) method using the wavelength dispersive XRF spectrometer (Axios mAX) with a 4 kW STmax160 X-ray tube with an Rh anode. The composition is shown in Table I. A fresh spot on the sample surface was chosen for each accumulation after 3000 laser shots. The integration time for one spectrum was 0.5 s. Plasma emission was collected by a 400 µm diameter fiber, which is coupled to a spectrograph (Andor Mechelle model ME5000) built with a gateable intensified charge-coupled device camera (iStar 334T from Andor Technology). Synchronization with the laser was performed using a digital delay generator (AtomTrace, AC-DDG-4 model). The gate time was fixed at 200 ns. All experiments were performed in ambient air (laboratory temperature in the range from 21 to 23 °C and humidity <20%). For each experimental set, the spectrograph was wavelength calibrated using a mercury calibration source (HG-2, Ocean Optics), and the relative efficiency correction was performed using a continuous halogen-deuterium lamp (DH-2000-BAL, Ocean Optics). Profilometry was performed using a laser confocal microscope (Olympus OLS5100) with a resolution of 0.012 µm using the 50× objective, the wavelength of the laser used was 405 nm, laser light receiving element—photomultiplier.

Results and Discussion

All plasma spectra were captured with a time gating window of 200 ns with a 50 ns delay step following the first registered plasma spectrum, until plasma emission was not present in

the measured spectra at ~ 1.5 µs. The plasma spectra of copper at different delay times are shown in Figure 2. The same spectral lines of Cu(I) are observed using both laser wavelengths, there are no spectral lines that would appear induced with only one of the wavelengths. At a 150 ns delay, the use of an IR laser wavelength results in a ~20% higher continuum and similar intensity lines. After 250 ns, a UV wavelength induces more intense Cu(I) 510.5, 515.3, and 521.8 nm spectral lines, and approximately the same intensity 570 and 578.2 nm lines. At 450 ns delay, UV laser wavelength-induced plasma produces a more intense signal across the full spectrum and continues to do so until plasma extinction. Spectra of steel at different delays are also shown in Figure 2. A higher (~400%) continuum is observed when using the IR laser wavelength. Plasma induced with both laser wavelengths displays similar intensity lines up to 750 ns, when the use of the UV laser wavelength results in more intense lines.

Plasma spectra on ceramics and glass samples are shown in Figure 3. On the *Y*-axis, the relative differences in intensities can be observed. The use of UV laser wavelength resulted in ~20 times higher amplitude of the signal as compared to IR laser wavelength-induced plasma. Most of the visible lines are calcium lines, which were used to calculate plasma temperature. With UV laser wavelength we were able to observe Ba (I) 611.08 nm and Ba(II) 614.17 nm spectral lines, which were not detectable using IR laser wavelength, as shown in Figure 3c. It is important to note that the amount of Ba

Table 1. Elemental composition of ceramics and glass samples, measured using the WDXRF method.

	Ceramics sample	Glass sample		Ceramics sample	Glass sample
Element	Composition (%)	Composition (%)	Element	Composition (%)	Composition (%)
O	41.861	30.527	Cr	0.015	0.133
Na	23.489	14.445	Fe	0.021	0.009
Mg	0.105	0.000	Ni	0.003	0.000
Al	7.340	0.135	Cu	0.177	0.107
Si	22.799	20.068	Rb	0.003	0.000
P	0.077	0.002	Sr	0.057	0.007
S	0.006	0.006	Zr	0.045	0.000
Cl	0.015	0.168	Ba	1.812	0.114
K	0.833	2.446	Ce	0.079	0.000
Ca	1.211	4.592	As	0.000	0.193
Ti	0.054	0.000			

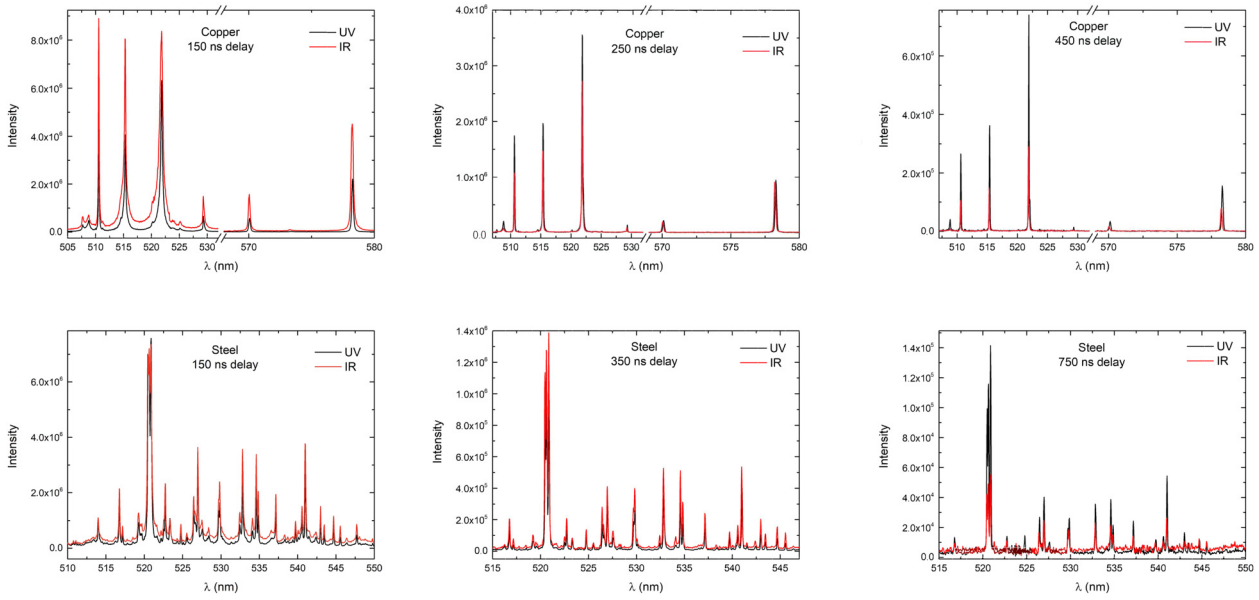

Figure 2. Comparison between the spectra of the plasma induced by the fs UV laser radiation (343 nm) and those induced by fs IR laser radiation (1030 nm) on copper (top) and steel (bottom) samples at different delay time.

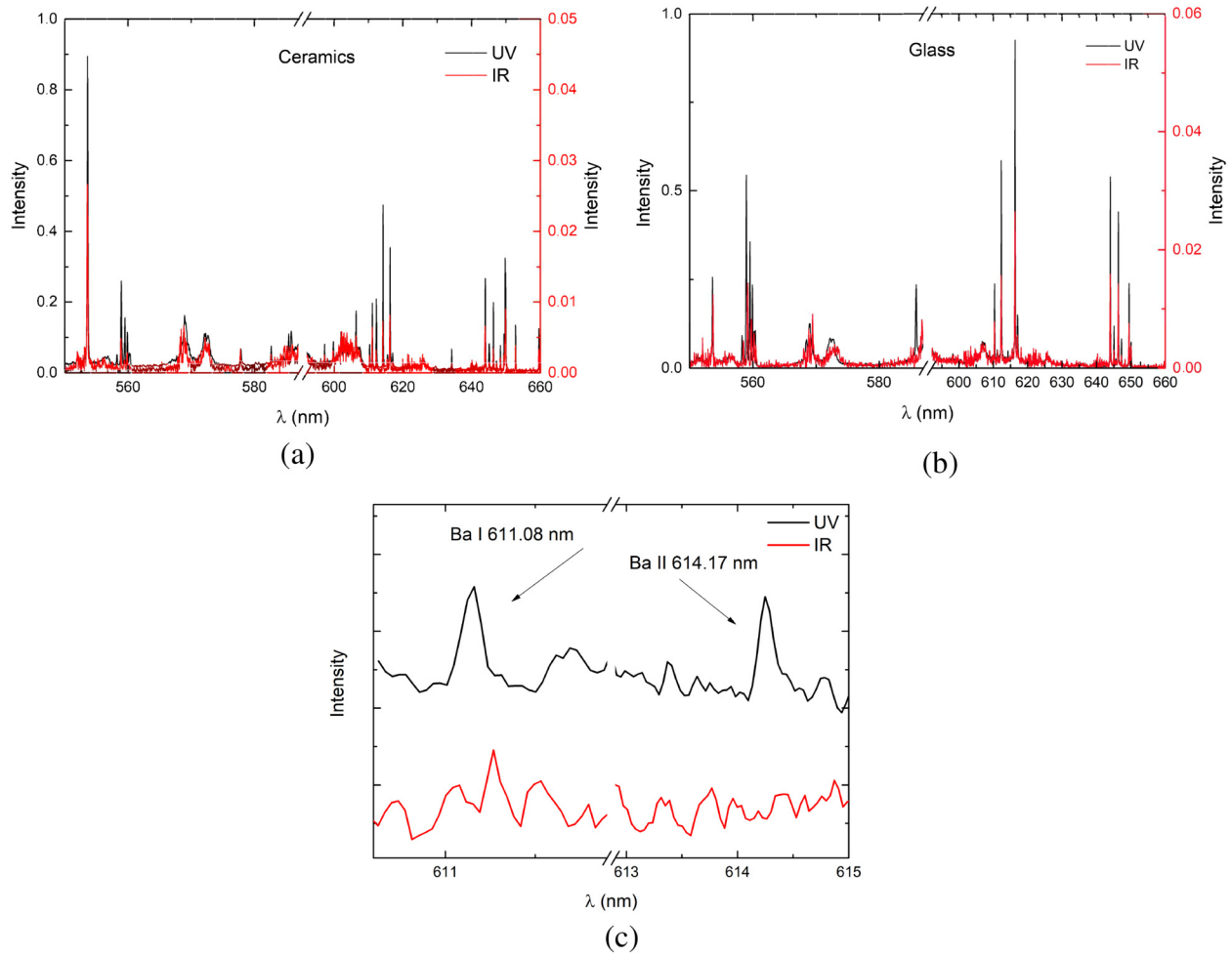

Figure 3. Comparison between the spectra of the plasma induced by the fs UV laser radiation (343 nm) and those induced by fs IR laser radiation (1030 nm) at 300 ns delay on a ceramics (a) and glass (b), and (c) shows a magnified spectrum region of interest on glass sample.

presented in the glass sample was very low and did not exceed 0.2%. Cr spectral lines were also detected.

Plasma temperature and electron density were determined by analyzing Cu(I), Fe(I), Ca(I), and K(I) emission lines, their spectroscopic data were obtained from the National Institute of Standards and Technology (NIST) database[34] and is shown in Tables II to IV. The plasma temperature was calculated using the Boltzmann plot method,[35] under the assumption of local thermodynamic equilibrium (LTE), which was verified through the McWhirter criterion, presented in Eq. 1:

$$n_e \geq 1.6 \times 10^{12} T_e^{1/2} (\Delta E)^3 \text{ cm}^{-3} \quad (1)$$

ΔE (eV) is the highest energy transition for which LTE exists and T_e (K) is the plasma temperature.[36] For a neutral plasma with transition energies of 3.2 eV for Fe, 3.8 eV for Cu,[37] and 4.34 eV for K,[38] and temperature of 6000–10 000 K, a plasma with electron density $\geq 9 \times 10^{15}$ cm^{-3} would satisfy this criterion for all samples.

Examples of Boltzmann plots obtained using 343 and 1030 nm laser wavelengths on copper, steel, glass, and ceramics samples are shown in Figure 4. The calculated excitation temperature values are the same, within error, for both used wavelengths on all samples investigated. Time-resolved plasma temperature is shown in Figure 5. The temperature on metal samples was in the range of 8000–11 000 K, on the glass sample it was in the vicinity of 4500–8000 K, and on ceramics it was 6000–11 000 K. The temperature uncertainty, according to El-Rabii et al.,[39] was expressed as

$$\frac{\Delta T}{T} = \frac{kT}{E' - E} \left| \frac{\Delta X}{X} \right| \quad (2)$$

where

$$\frac{\Delta X}{X} = \frac{\Delta I}{I} + \frac{\Delta I'}{I} + \frac{\Delta A}{A} + \frac{\Delta A'}{A} \quad (3)$$

where A is the Einstein coefficient, I is the intensity of the line, and $E' - E$ is the difference in upper energy state

Table II. Spectroscopic parameters of Cu(I) emission lines used to calculate plasma parameters, taken from the NIST database.[33]

	Energies (eV)			Transitions	
Wavelength of Cu I (nm)	E_i	E_k	Transition probability (g_kA_{ki})($10^7 s^{-1}$)	Upper level	Lower level
510.55	1.389	3.817	0.8	$3d^{10}4p$	$3d^94s^2$
515.32	3.786	6.191	24	$3d^{10}4d$	$3d^{10}4p$
521.82	3.817	6.192	45	$3d^{10}4d$	$3d^{10}4p$
570.02	1.642	3.817	0.01	$3d^{10}4p$	$3d^94s^2$
578.21	1.642	3.786	0.33	$3d^{10}4p$	$3d^94s^2$

Table III. Spectroscopic parameters of Fe(I) emission lines used to calculate plasma parameters, taken from the NIST database.[33]

	Energies (eV)				Transitions
Wavelength of Fe I (nm)	E_i	E_k	Transition probability (g_kA_{ki})($10^7 s^{-1}$)	Upper level	Lower level
527.04	1.608	3.960	1.1	$3d^6(^5D)4s4p(^3P^\circ)$	$3d^7(^4F)4s$
537.15	0.958	3.266	0.53	$3d^6(^5D)4s4p(^3P^\circ)$	$3d^7(^4F)4s$
541.09	4.473	6.764	57	$3d^7(^4F)4d$	$3d^7(^4F)4p$
542.97	0.958	3.241	0.3	$3d^6(^5D)4s4p(^3P^\circ)$	$3d^7(^4F)4s$
544.69	0.990	3.266	0.27	$3d^6(^5D)4s4p(^3P^\circ)$	$3d^7(^4F)4s$
613.77	2.588	4.608	0.7	$3d^7(^4F)^4p$	$3d^64s^2$

Table IV. Spectroscopic parameters of Ca(I) and K(I) emission lines used to calculate plasma parameters on glass and ceramics samples, taken from the NIST database.[33]

	Energies (eV)				Transitions
Wavelength of Ca(I) (nm)	E_i	E_k	Transition probability (g_kA_{ki})($10^7 s^{-1}$)	Upper level	Lower level
527.03	2.526	4.878	25	$3p^63d4p$	$3p^63d4s$
558.88	2.526	4.744	34	$3p^63d4p$	$3p^63d4s$
610.27	1.879	3.910	2.9	$3p^64s5s$	$3p^64s4p$
612.22	1.886	3.910	8.6	$3p^64s5s$	$3p^64s4p$
616.22	1.899	3.910	14	$3p^64s5s$	$3p^64s4p$
Wavelength of K(I) (nm)	E_i	E_k	Transition probability (g_kA_{ki})($10^7 s^{-1}$)	Upper level	Lower level
769.90	0.000	1.610	7.5	$3p^64p$	$3p^64s$

(~2.4 eV for Cu, ~3.5 eV for Fe, and ~1 eV when Ca lines are used on glass and ceramics samples). The uncertainty on copper sample was ~11%, on steel sample ~5%, on ceramic sample, and on glass sample ~28%.

Electron density was calculated from the Stark-broadened profile of Cu(I), Fe(I), and K(I) lines using Eq. 4:[40]

$$n_e = \frac{\Delta\lambda_{1/2} \times 10^{16}}{2\omega} \quad (4)$$

where ω is the electron impact parameter, n_e is the electron density and $\Delta\lambda_{(1/2)}$ is the full width half-maximum (FWHM) of the emission profile fitted to a Lorentzian profile. The values of ω were taken from Zmerli et al.[41] for Cu(I) 510.5 nm spectral line, Konjević and Wiese[42] for Fe(I) 541.09 nm line and Lesage[43] for K(I) 769.9 nm line. Electron density as a function of delay for 343 nm and 1030 nm laser wavelengths is shown in Figure 6. The spectra were acquired using a 200 ns gate window and delay in the range of 150–1100 ns for metals and 100–2300 ns for ceramics and glass, which are sufficient for the establishment of LTE and a significant reduction in the intensity of the bremsstrahlung emission. There is no obvious impact of the laser wavelength used on the electron density of the plasma. Electron density on copper was in the range of $(1-1.6) \times 10^{18}$ cm^{-3}, on steel it was 8×10^{15}–2×10^{16} cm^{-3}, on glass and ceramics it was within the range of 8×10^{15}–1.9×10^{16} cm^{-3}. The uncertainty in the determination of the electron density was ~30% on copper sample, ~35% on steel sample, and ~25% on ceramics

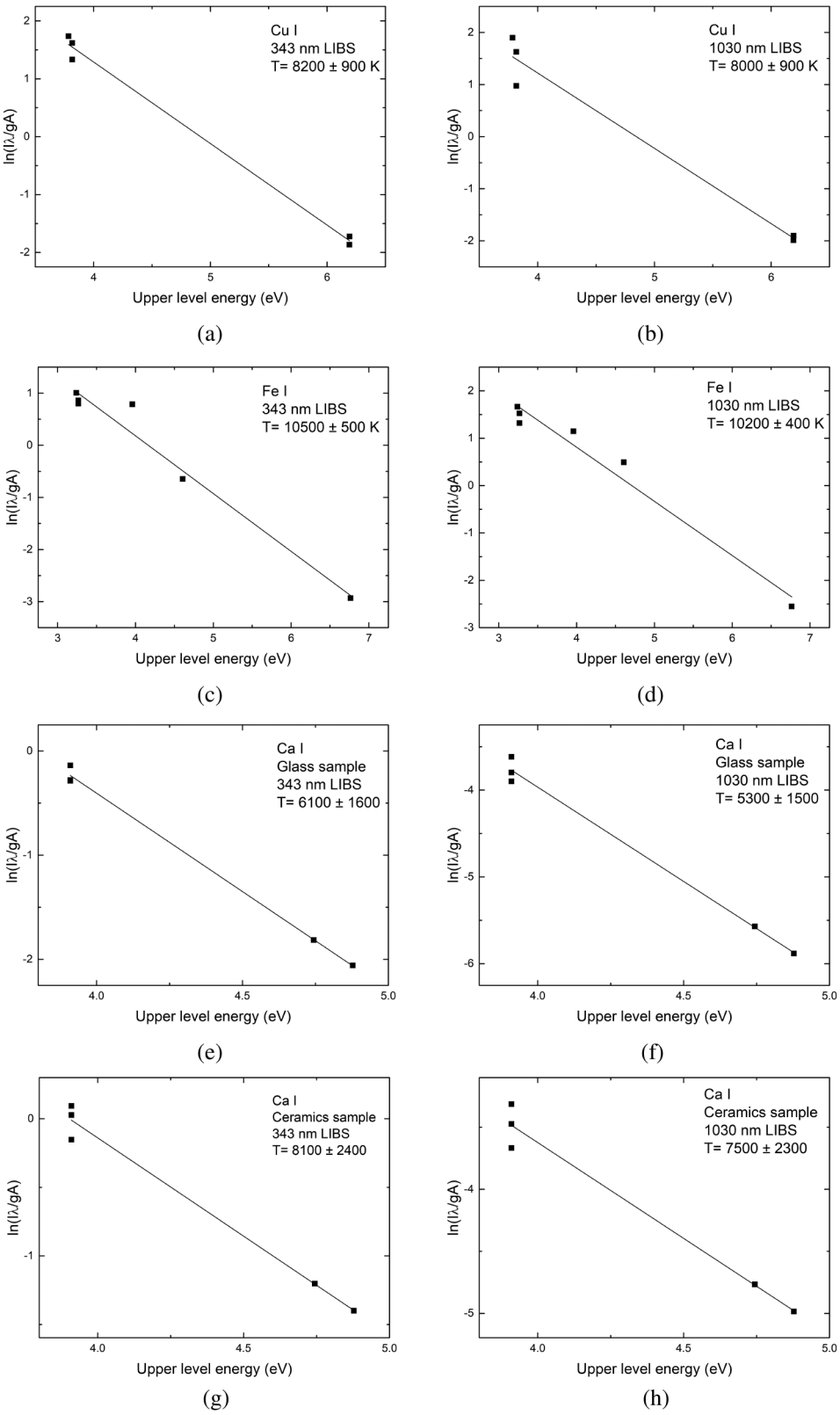

Figure 4. Boltzmann plots for the calculation of plasma temperature of Cu(I) (a, b), Fe(I) (c, d), Ca(I) on glass (e, f), and ceramics (g, h) samples.

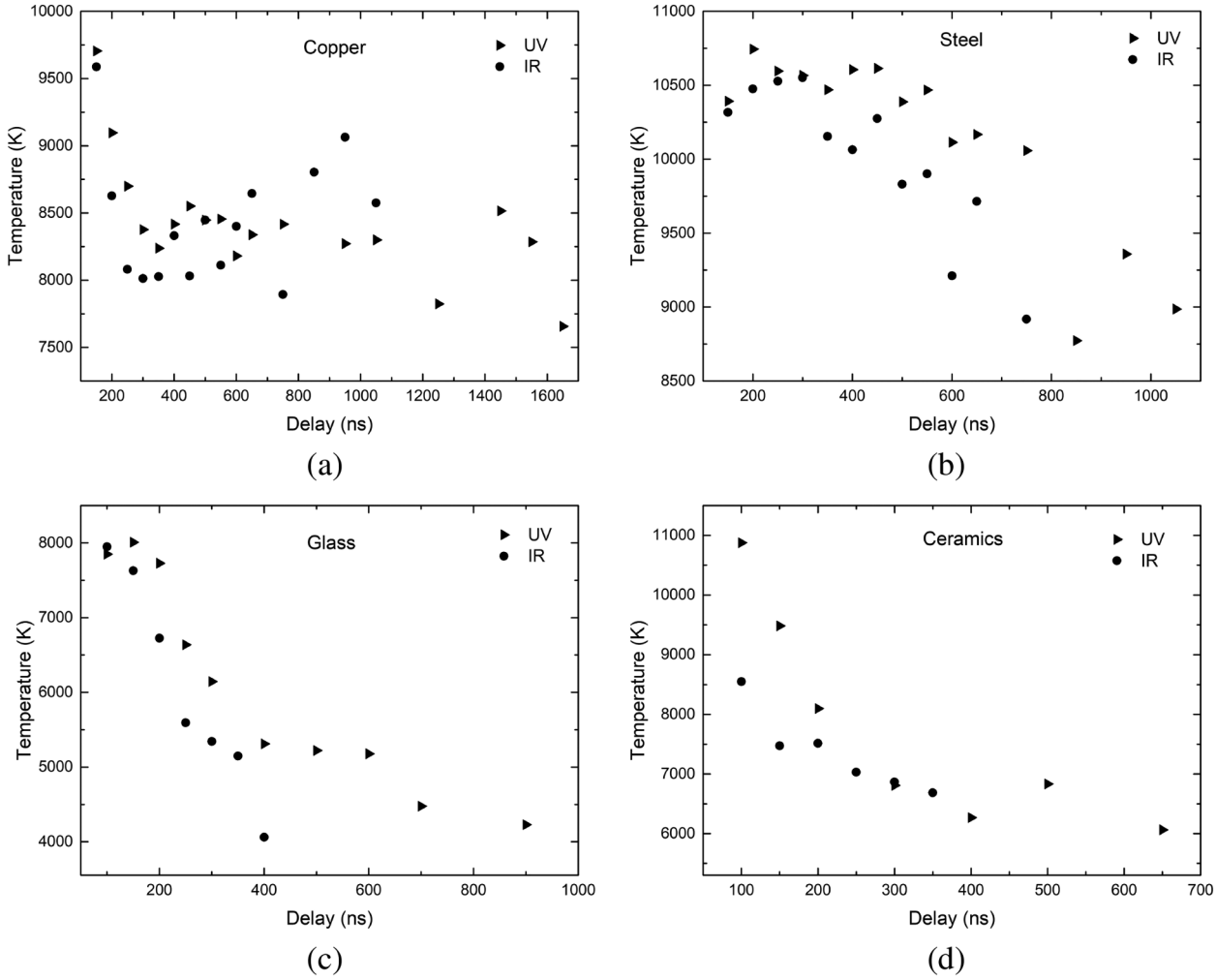

Figure 5. Time-resolved plasma temperature for fs-LIBS on copper (a), steel (b), glass (c), and ceramics (d) samples for 343 nm (UV) and 1030 nm (IR) wavelengths.

and glass samples, taking into account the uncertainties of the FWHM measurement, the electron impact parameter, and the linewidth's de-convolution to the instrumental width. The possibility of electron density error due to temperature uncertainty was also investigated, but it was found to be negligible.

Signal-to-noise ratio (SNR) was also evaluated for both wavelengths used on all samples, i.e., Cu(I) 521.82 nm, Fe(I) 541.09 nm, and Ca(I) 612.22 nm on glass and ceramics samples, and is shown in Figure 7. The use of the UV laser wavelength resulted in significantly higher SNR on all samples: copper (~100% higher), steel (~300% higher), glass (~400% higher), and ceramics (~40% higher). Plasma lifetime was evaluated by fitting an exponential decay function to the temporal evolution of the integrated intensity of the plasma emission lines and determining the rate of decay τ. The τ coefficient was increased on all samples with the use of the UV laser wavelength. On the glass sample, it was 98 ± 4 ns using UV and 74 ± 5) ns using IR laser wavelengths. On the ceramic sample, it was 107 ± 5 ns for UV and 88 ± 7 ns for IR laser wavelengths. On the copper sample, it was 61 ± 2 ns using UV and 37 ± 0.4 ns using IR laser wavelengths. On the steel sample, it was 68 ± 4 ns using UV and 58 ± 5 ns using IR laser wavelengths.

The ablated volume on all samples was investigated using a 3D laser scanning microscope (Olympus OLS5100). On the copper sample, it was $\sim(110 \pm 6) \times 10^3\ \mu m^3$ following UV laser wavelength ablation and $\sim(14 \pm 1.5) \times 10^3\ \mu m^3$ using the IR laser wavelength. On the steel sample, it was $\sim(36 \pm 3.5) \times 10^3\ \mu m^3$ using the UV laser wavelength and $\sim(5 \pm 1.5) \times 10^3\ \mu m^3$ using the IR laser wavelength. On the ceramics sample, the ablation volume was $\sim(82 \pm 1) \times 10^3\ \mu m^3$ using the UV laser wavelength and $\sim(70 \pm 1.5) \times 10^3\ \mu m^3$ using the IR laser wavelength. On the glass sample, it

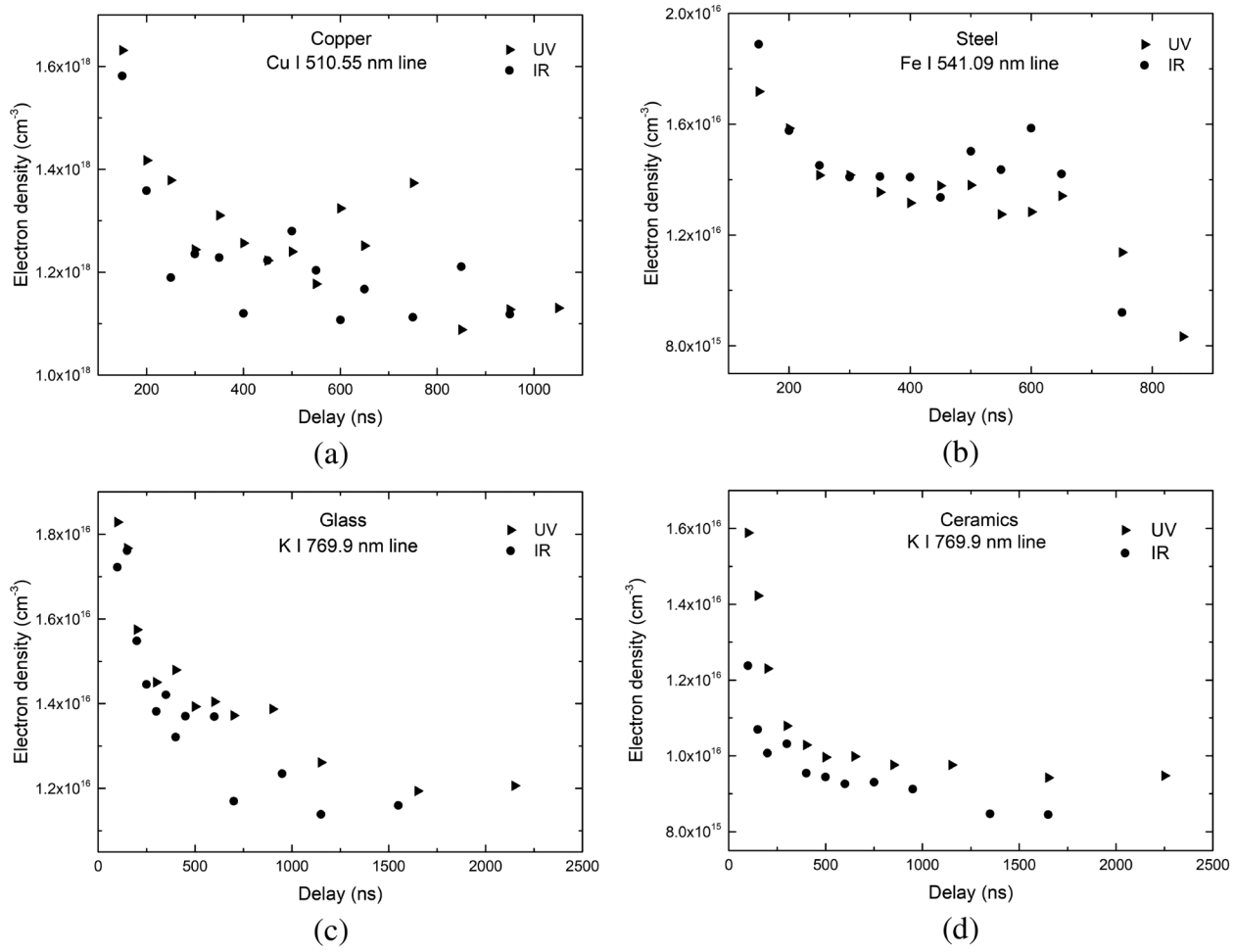

Figure 6. Time-resolved electron density for fs-LIBS for UV and IR laser wavelengths using Cu(I) (a) 510.5 nm, Fe(I) (b) 541.1 nm, and K(I) (c, d) spectral lines on copper, steel, glass, and ceramics samples, respectively.

was $\sim(76 \pm 1) \times 10^3\ \mu m^3$ using the UV wavelength and $\sim(13 \pm 1) \times 10^3\ \mu m^3$ using the IR laser wavelength. Different energies were used on different samples, but the fluence was kept constant between the wavelengths. On all samples, the UV wavelength ablated a larger volume of material by approximately eight times on copper and steel samples, by approximately six times on the glass sample and by ~20% on the ceramics sample. In our opinion, the main mechanisms leading to the growth of SNR in the UV range are increased multi-photon ionization when plasma is induced by UV radiation, higher nonlinearity, and higher linear absorption of the material in the UV range. Moreover, the lower background in the case of UV laser-induced plasma was observed. Since the main background continuum in LIBS is caused by the Bremsstrahlung radiation,[35] and it is known that inverse Bremsstrahlung absorption is proportional to λ^2,[44] the continuum background is higher for IR laser-induced plasma.

Conclusion

In this work, we investigated the effect of a fs laser wavelength (1030 and 343 nm) at fixed energy fluence on the observed copper, steel, ceramics, and glass plasma parameters using the LIBS technique. The evaluated plasma temperature and electron density did not show any strong dependence on laser wavelength for all the samples and coincided with the limits of error. However, the SNR significantly increased using UV laser radiation for all samples: copper (~100%), steel (~300%), glass (~400%), and ceramics (~40%). The UV laser wavelength, unlike the IR laser wavelength, allows us to detect the spectral lines of the elements whose concentration in the sample is <0.2% (e.g., Ba and Cr lines in the glass sample). It was evaluated that fs UV laser radiation significantly increased the ablated material volume on all the samples, which, together with the increased multi-photon ionization efficiency and decreased continuum background radiation at shorter

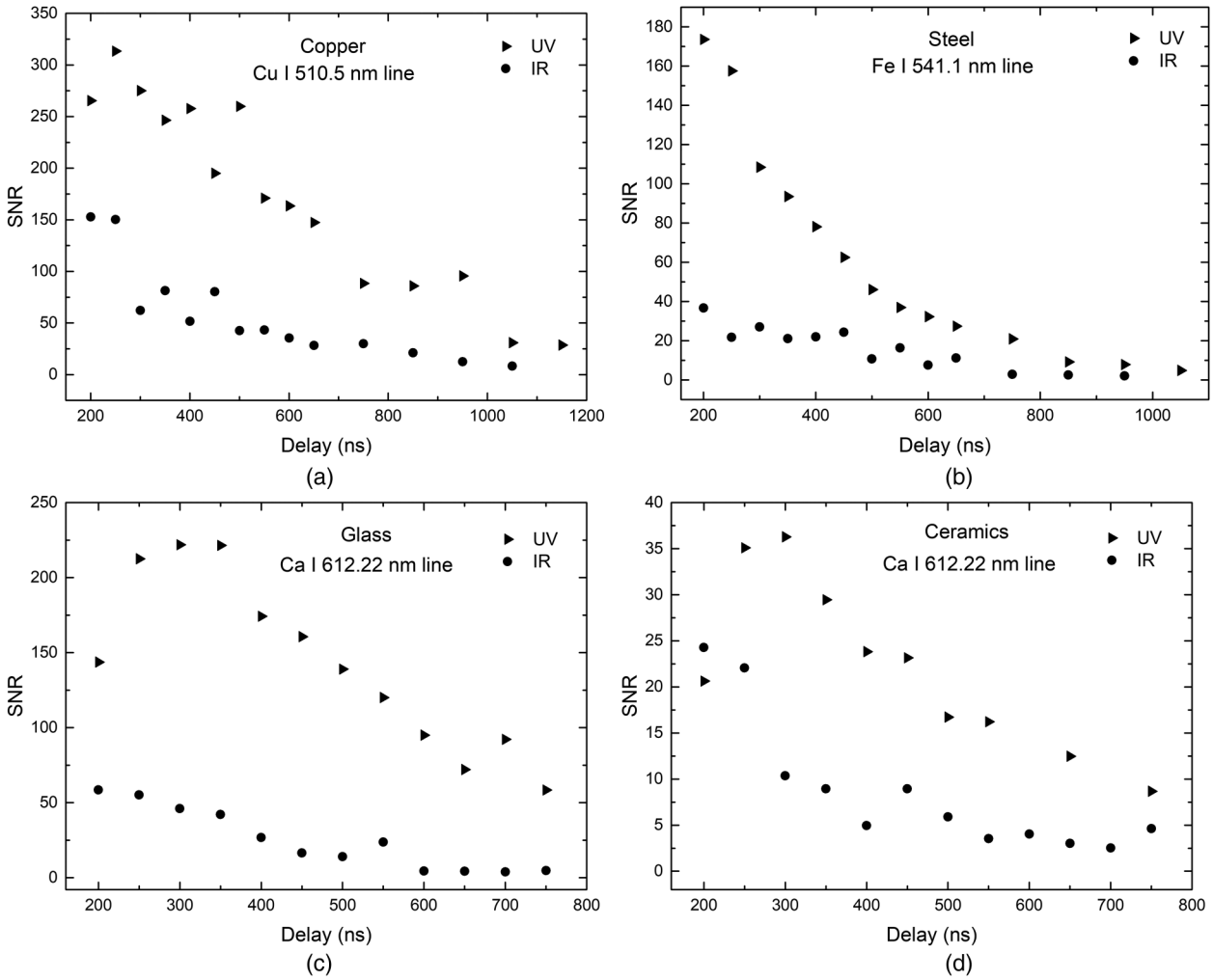

Figure 7. Signal-to-noise ratio (SNR) evolution as a function of delay for Cu(I) (a), Fe(I) (b), and Ca(I), (c, d) on copper, steel, glass, and ceramics samples, respectively.

wavelengths for the fs pulses, led to an increase in SNR using UV laser radiation. The results obtained confirmed that using fs UV laser wavelength for laser-induced breakdown spectroscopy experiments can significantly enhance SNR and therefore the limit of detection for certain materials.

Declaration of Conflicting Interests

The authors declared no potential conflicts of interest with respect to the research, authorship, and/or publication of this article.

Funding

The authors disclosed receipt of the following financial support for the research, authorship, and/or publication of this article: This work has received funding from the European Regional Development Fund (project 01.2.2-LMT-K-718-03-0029) under a grant agreement with the Research Council of Lithuania (LMTLT).

ORCID iDs

Gytis Zaremba https://orcid.org/0009-0007-8895-144X
Ona Balachninaite https://orcid.org/0000-0002-0433-3975

References

1. A. Santagata, R. Teghil, G. Albano, D. Spera, et al. "Fs/ns Dual-Pulse LIBS Analytic Survey for Copper-Based Alloys". Appl. Surf. Sci. 2007. 254(4): 863–867.
2. T.A. Labutin, V.N. Lednev, A.A. Ilyin, A.M. Popov. "Femtosecond Laser-Induced Breakdown Spectroscopy". J. Anal. At. Spectrom. 2016. 31(1): 90–118.
3. C. Donnet, J. Granier, G. Vergé, Y. Bleu, et al. "2D Reproduction of the Face on the Turin Shroud by Infrared Femtosecond Pulse Laser Processing". Appl. Opt. 2019. 58(9): 2158–2165.
4. A. De Bonis, B. De Filippo, A. Galasso, A. Santagata, et al. "Comparison of the Performances of Nanosecond and Femtosecond Laser-Induced Breakdown Spectroscopy for Depth Profiling of an Artificially Corroded Bronze". Appl. Surf. Sci. 2014. 302: 275–279.

5. K.C. Hartig, J. Colgan, D.P. Kilcrease, J.E. Barefield, et al. "Laser-Induced Breakdown Spectroscopy Using Mid-Infrared Femtosecond Pulses". J. Appl. Phys. 2015. 118: 043107.
6. P. Qi, W. Qian, L. Guo, J. Xue, et al. "Sensing with Femtosecond Laser Filamentation". Sensors. 2022. 22(18): 7076.
7. H.L. Xu, P.T. Simard, Y. Kamali, J.F. Daigle, et al. "Filament-Induced Breakdown Remote Spectroscopy in a Polar Environment". Laser Phys. 2012. 22(12): 1767–1770.
8. S.L. Chin, H.L. Xu, Q. Luo, F. Théberge, et al. "Filamentation 'Remote' Sensing of Chemical and Biological Agents/Pollutants Using Only One Femtosecond Laser Source". Appl. Phys. B. 2009. 95(1): 1–12.
9. S. Tzortzakis, D. Anglos, D. Gray. "Ultraviolet Laser Filaments for Remote Laser-Induced Breakdown Spectroscopy (LIBS) Analysis: Applications in Cultural Heritage Monitoring". Opt. Lett. 2006. 31(8): 1139–1141.
10. W. Liu, H.L. Xu, G. Méjean, Y. Kamali, et al. "Efficient Non-Gated Remote Filament-Induced Breakdown Spectroscopy of Metallic Sample". Spectrochim. Acta, Part B. 2007. 62(1): 76–81.
11. M. Baudelet, M. Richardson, M. Sigman. "Self-Channeling of Femtosecond Laser Pulses for Rapid and Efficient Standoff Detection of Energetic Materials". In: 2009 IEEE Conference on Technologies for Homeland Security (HST). Waltham, Massachusetts; 11–12 May 2009. Pp. 472–476.
12. A.K. Shaik, N.R. Epuru, H. Syed, C. Byram, et al. "Femtosecond Laser-Induced Breakdown Spectroscopy Based Standoff Detection of Explosives and Discrimination Using Principal Component Analysis". Opt. Express. 2018. 26(7): 8069.
13. A. Baskevicius, O. Balachninaite, M. Karpavicius, S. Butkus, et al. "Monitoring of The Femtosecond Laser Micromachining Process of Materials Immersed in Water by Use of Laser-Induced Breakdown Spectroscopy". J. Laser Micro/Nanoeng. 2016. 11(3): 381–387.
14. H.L. Xu, J. Bernhardt, P. Mathieu, G. Roy, et al. "Understanding the Advantage of Remote Femtosecond Laser-Induced Breakdown Spectroscopy of Metallic Targets". J. Appl. Phys. 2007. 101(3): 033124-033124-6.
15. D. Díaz, A. Molina, D. Hahn. "Effect of Laser Irradiance and Wavelength on The Analysis of Gold- And Silver-Bearing Minerals with Laser-Induced Breakdown Spectroscopy". Spectrochim. Acta, Part B. 2018. 145: 86–95.
16. C. Barnett, E. Cahoon, J.R. Almirall. "Wavelength Dependence on The Elemental Analysis of Glass By Laser-Induced Breakdown Spectroscopy". Spectrochim. Acta, Part B. 2008. 63(10): 1016–1023.
17. M.A. Kasem, J.J. Gonzalez, R.E. Russo, M. Abdel Harith, et al. "Effect of The Wavelength on Laser-Induced Breakdown Spectrometric Analysis of Archaeological Bone". Spectrochim. Acta, Part B. 2014. 101(1): 26–31.
18. H. Cui, Y. Tang, S. Ma, M. Shixiang, Y. Ma, et al. "Influence of Laser Wavelength on Self-Absorption Effect in Laser-Induced Breakdown Spectroscopy". Optik. 2020. 204: 164144.
19. S. Amoruso, M. Armenante, V. Berardi, R. Bruzzese, et al. "Absorption and Saturation Mechanisms in Aluminium Laser Ablated Plasmas". Appl. Phys. A. 1997. 65(3): 265–271.
20. E. Tognoni, V. Palleschi, M. Corsi, G. Cristoforetti. "Quantitative Micro-Analysis by Laser-Induced Breakdown Spectroscopy: A Review of the Experimental Approaches". Spectrochim. Acta, Part B. 2002. 57(7): 1115–1130.
21. X.L. Mao, A.C. Ciocan, O.V. Borisov, R.E. Russo. "Laser Ablation Processes Investigated Using Inductively Coupled Plasma-Atomic Emission Spectroscopy (ICP-AES)". Appl. Surf. Sci. 1998. 127–129: 262–268.
22. M.S. Qaisar, G.J. Pert. "Laser Ablation of Mg, Cu, and Pb Using Infrared and Ultraviolet Low-Fluence Lasers". J. Appl. Phys. 2003. 94: 1468–1477.
23. A. Semerok, C. Chaléard, V. Detalle, J.-L. Lacour, et al. "Experimental Investigations of Laser Ablation Efficiency of Pure Metals with Femto, Pico and Nanosecond Pulses". Appl. Surf. Sci. 1999. 138(1): 311–314.
24. L.M. Cabalin, J.J. Laserna. "Experimental Determination of Laser-Induced Breakdown Thresholds of Metals Under Nanosecond Q-Switched Laser Operation". Spectrochim. Acta, Part B. 1998. 53(5): 723–730.
25. W. Sdorra, J. Brust, K. Niemax. "Basic Investigations for Laser Microanalysis: IV. The Dependence on The Laser Wavelength in Laser Ablation". Mikrochim. Acta. 1992. 108(1–2): 1–10.
26. G. Abdellatif, H. Imam. "A Study of The Laser Plasma Parameters At Different Laser Wavelengths". Spectrochim. Acta, Part B. 2002. 57: 1155–1165.
27. T.E. Jeffries, N.J.G. Pearce, W.T. Perkins, A. Raith. "Chemical Fractionation During Infrared and Ultraviolet Laser Ablation Inductively Coupled Plasma Mass Spectrometry–Implications for Mineral Microanalysis". Anal. Commun. 1996. 33(1): 35–39.
28. D. Figg, M.S. Kahr. "Elemental Fractionation of Glass Using Laser Ablation Inductively Coupled Plasma Mass Spectrometry". Appl. Spectrosc. 1997. 51(8): 1185–1192.
29. N. Huber, R. Viskup, T. Linsmeyer, H. Scherndl, et al. "Detection of Heavy Metals in Waste Polymers by Laser-Induced Breakdown Spectroscopy: a Comparison of UV and IR Lasers As Ablation Source". Opt. Sens. Detect. 2010. 7726: 77260G.
30. L. Fornarini, V. Spizzichino, F. Colao, R. Fantoni, et al. "Influence of Laser Wavelength on LIBS Diagnostics Applied to the Analysis of Ancient Bronzes". Anal. Bioanal. Chem. 2006. 385 (2): 272–280.
31. S. Messaoud Aberkane, A. Bendib, K. Yahiaoui, et al. "Effect of Laser Wavelength on The Correlation Between Plasma Temperature and Surface Hardness of Fe–V–C Metallic Alloys". Spectrochim. Acta, Part B. 2015. 113: 147–151.
32. M. Fikry, W. Tawfik, M.M. Omar. "Investigation on The Effects of Laser Parameters on The Plasma Profile of Copper Using Picosecond Laser-Induced Plasma Spectroscopy". Opt. Quantum Electron. 2020. 52(5): 249.
33. J.M. Liu. "Simple Technique for Measurements of Pulsed Gaussian-Beam Spot Sizes". Opt. Lett. 1982. 7(5): 196–198.
34. A. Kramida, Y. Ralchenko, J. Reader, NIST ASD Team. "NIST Atomic Spectra Database: NIST Standard Reference Database 78 Version 5.11". https://www.nist.gov/pml/atomic-spectra-database [accessed Mar 18 2024].
35. H.R. Griem. Plasma Spectroscopy: Spectral Line Broadening by Plasmas. New York: Academic Press Inc., 1974.
36. E. Tognoni, V. Palleschi, M. Corsi, G. Cristoforetti, et al. "From Sample to Signal in Laser-Induced Breakdown Spectroscopy: A Complex Route to Quantitative Analysis". In: Miziolek AW, Palleschi V, Schechter I, editors. Laser Induced Breakdown Spectroscopy. Cambridge: Cambridge University Press, 2006. Pp. 122-170.

37. G. Cristoforetti, A. De Giacomo, M. Dell'Aglio, S. Legnaioli, et al. "Local Thermodynamic Equilibrium in Laser-Induced Breakdown Spectroscopy: Beyond the McWhirter Criterion". Spectrochim. Acta B: At. Spectrosc. 2010. 65: 86–95.
38. J. Sugar, C. Corliss. Atomic Energy Levels of The Iron-Period Elements: Potassium Through Nickel. New York: American Institute of Physics for the National Bureau of Standard, 1985.
39. H. El-Rabii, S.B. Victorov, A.P. Yalin. "Properties of an Air Plasma Generated by Ultraviolet Nanosecond Laser Pulses". J. Phys. D. 2009. 42(7): 075203.
40. G. Bekefi, H. Reed Allan. "Principles of Laser Plasmas". J. Electrochem. Soc. 1977. 124: 435C.
41. B. Zmerli, N. Ben Nessib, M.S. Dimitrijević, S. Sahal-Brechot, et al. "Stark Broadening Calculations of Neutral Copper Spectral Lines and Temperature Dependence". Phys. Scr. 2010. 82(5): 055301.
42. N. Konjević, W.L. Wiese. "Experimental Stark Widths and Shifts for Spectral Lines of Neutral and Ionized Atoms". J. Phys. Chem. 1990. 19: 1307–1385.
43. A. Lesage. "Experimental Stark Widths and Shifts for Spectral Lines of Neutral and Ionized Atoms: A Critical Review of Selected Data for the Period 2001–2007". New Astron. Rev. 2009. 52(11-12): 471–535.
44. J. Yu, Q. Ma, V. Motto-Ros, X. Wang, X. Bai. "Generation and Expansion of Laser-Induced Plasma as a Spectroscopic Emission Source". Front. Phys. 2012. 7(6): 649–669.